GEOFLUIDS

Geofluids (2016) doi: 10.1111/gfl.12184

Injection-induced seismicity in Carbon and Emery Counties, central Utah

M. R. M. BROWN AND M. LIU

Department of Geological Sciences, University of Missouri, Columbia, MO, USA

ABSTRACT

Utah is one of the top producers of oil and natural gas in the United States. Over the past 18 years, more than 4.2 billion gallons of wastewater from the petroleum industry has been injected into the Navajo Sandstone, Kayenta Formation, and Wingate Sandstone in Carbon and Emery Counties, central Utah, where seismicity has increased during the same period. Previous studies have attributed this seismicity to coal mining. Here, we present evidence for wastewater injection being a major cause of the increased seismicity. We show that, in the coal mining area, seismicity rate increased significantly 1–5 years following the wastewater injection, and the earthquakes, mostly with magnitudes <3.0, are concentrated in areas seismically active prior to the injection. Using simple analytical and numerical models, we show that the injection in central Utah can sufficiently raise pore pressure to trigger seismicity within 10–20 km of the injection wells, and the time needed for the diffusion of pore pressure may explain the observed lag of seismicity increase behind the commencement of injection. The *b*-value of these earthquakes increased following the wastewater injection, which is consistent with these events being injection-induced. We conclude that the marked increase in seismicity rate in central Utah is induced by both mining activity and wastewater injection, which raised pore pressure along preexisting faults.

Key words: *b*-value, injection-induced seismicity, pore pressure, wastewater injection

Received 20 November 2015; accepted 5 July 2016

Corresponding author: Megan R. M. Brown, University of Colorado Boulder, UCB 399, Boulder, CO 80309-0399, USA.
Email: Megan.R.Brown@colorado.edu. Tel: +303 492 8141. Fax: +303 492 2606.
and
Mian Liu, Department of Geological Sciences, University of Missouri, 101 Geology Building, Columbia, MO 65211-1380, USA.
Email: lium@missouri.edu. Tel: +573 882 3784. Fax: +573 882 5458.

INTRODUCTION

Induced seismicity refers to earthquakes caused by mining, water impoundment in reservoirs, and fluid injection (National Research Council of the National Academies 2013). A long-recognized phenomenon, induced seismicity has stirred up widespread public concerns in recent years; the increased fluid injection associated with hydrocarbon production has been linked to marked increase in seismicity in many states such as Oklahoma (Ellsworth 2013; Keranen *et al.* 2013), and studies have suggested that larger volumes of injection can induce bigger earthquakes (McGarr 2014).

Utah is one of the top states for hydrocarbon production in the nation. Injection of wastewater began in the mid-1980s in central Utah, with consistent large volumes of wastewater injection commencing in the mid-1990s (UIC public record well files). As of May 2013, over 399 million barrels (4.56×10^7 m^3) of wastewater has been injected in central Utah. Seismicity rate in central Utah increased significantly during the same period.

Previous studies have attributed the area's seismicity to coal mining (Smith *et al.* 1974; Arabasz *et al.* 2007; Pechmann *et al.* 2008), which has been extensive in central Utah. Mining induced seismicity (MIS) in central Utah has been monitored by the University of Utah Seismograph Station (UUSS) regional network since 1978 (Kubacki *et al.* 2014). The MIS is mostly a result of underground mine collapse and shear-slip motion on rock fractures (Pechmann *et al.* 2008). Most of the MIS is smaller than magnitude 3 and close to the mine depth, which is less than 960 m (Arabasz *et al.* 2007).

Is the increased seismicity in central Utah caused entirely by mining activity? Or is it induced by the wastewater injection? Does the increased seismicity share the characteristics of injection-induced seismicity (i.e., small events on preexisting faults (Ellsworth 2013))? To address these questions, we explored the spatiotemporal correlations between the seismicity, wastewater injection, and coal mining activity in central Utah. In addition, we tested the viability of triggering the increased seismicity by elevated pore pressure from the injection. Finally, we calculated the temporal variation in *b*-values to determine temporal changes in the differential stress of the area and examine changes in magnitude distribution of the events.

DATA

Wastewater injection data

Currently, the US Environmental Protection Agency's (EPA) Underground Injection Control (UIC) program governs all injection wells, including Class II injection wells, which are used to inject nonhazardous waste fluids that are by-products of oil and natural gas production or storage of fluids used for enhanced recovery of oil or natural gas. Often, state agencies administer the UIC program for the EPA, and Utah has administered the program since 1983. Utah's Department of Natural Resources (DNR), Division of Oil, Gas and Mining (DOGM) regulates all operations related to the production of oil or natural gas, including the UIC program.

In Utah, service wells include all Class II injection well designations (Fig. 1): water injection wells used in enhanced recovery, waste water disposal wells, and gas injection wells. Service wells also include water supply wells, which are pumping wells. Many of the records for the wells are public record and available online through a searchable database. Injection volume data for the wastewater disposal wells is available from 1986 to the present. UIC permitting requires reporting of monthly well injection volumes and maximum injection pressure. Fig. 1A shows four areas of clustered injection wells that are targets of this study. The areas were chosen based solely on the location of the injection wells.

Seismic data

The study areas are located within or near the Intermountain Seismic Belt (Fig. 1A). Focal mechanisms show predominantly WNW-ESE extension (Arabasz *et al.* 2007). Maximum focal depths of the natural seismicity are 15–25 km; however, focal depths are well constrained only for a small fraction of the events because of insufficient coverage of seismic stations (Arabasz *et al.* 2007).

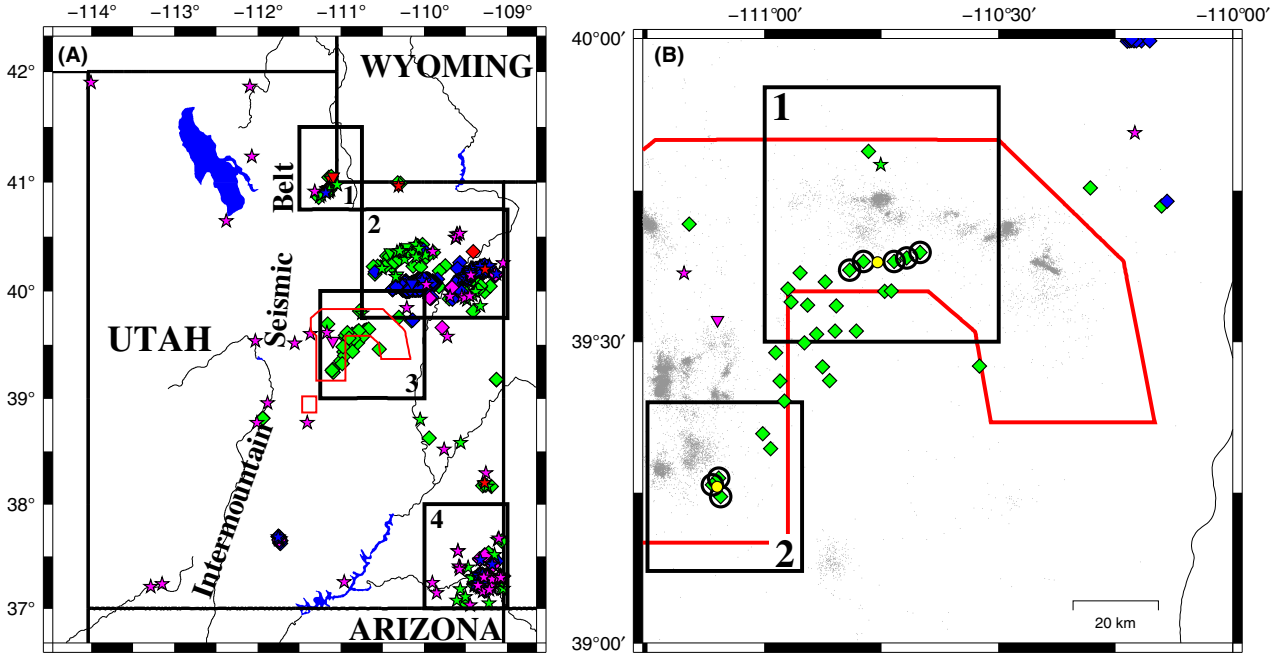

Fig. 1. Study areas and service well locations. Service well locations, from Utah's DNR, Division of Oil, Gas and Mining, are represented by the diamonds (active wells), inverted triangles (inactive wells), and stars (abandoned wells) with red = gas injection wells; blue = water injection wells; purple = water supply wells; and green = wastewater disposal wells. Red polygons outline the areas of active coal mining. (A) Boxes 1–4 show the areas chosen for study based on the well locations; (B) Area 3 enlarged with seismicity since 1981 in gray dots (magnitudes range from −0.84 to 5.17), from the USGS ComCat Search (http://earthquake.usgs.gov/earthquakes/search/), and service well locations. Area 3's Clusters 1 and 2 are boxed and labeled. Well locations with black circles are wells of interest, and yellow filled circles mark the center location of the wells of interest.

In this study, we use the seismic data from the United States Geological Survey (USGS) (http://earthquake.usgs.gov/earthquakes/search/); most of the records are from the UUSS network that began digital recording on January 1, 1981 (Arabasz *et al.* 2007). Magnitudes in the catalog (ranging from $M < 0$ to M5.17) are mostly based on local magnitude (M_L) scales and coda magnitude scales (M_c), which is an empirical estimate of local magnitude. Comparisons of revised magnitudes to moment magnitudes (M_w) show that the M_L magnitudes are almost equivalent to M_w magnitudes (Pechmann *et al.* 2007). Quarry blasts and other artificial seismic events are routinely identified and removed from the UUSS catalog based on the character of the recorded waveform and information on the location and time of day of the event (Arabasz *et al.* 2007).

From October 2000 through April 2001, the University of Utah installed a temporary seismic array in Emery County, Utah, to evaluate the effects of the MIS on a nearby reservoir. Relocation of seismic events collected from this array indicates that most were located at depths <1 km and within ±0.6 km of mine level (Arabasz *et al.* 2002). Almost all of the 1829 relocated seismic events were located within Area 3 (Fig. 1). We compared the times of the 1829 relocated seismic events and found only 1784 of the events were included in our data set. Because Arabasz *et al.* (2002) confirmed their data set of seismic events to be MIS using relocation techniques, we removed the 1784 events that were in both data sets to assure this seismicity was not the cause of the increased seismicity; the increased rate remained. Therefore, the Arabasz *et al.* (2002) data were included in our data set for the comparisons and calculations to evaluate the occurrence of mining and injection-induced seismicity.

CHANGE OF SEISMICITY RATES

To determine whether the seismicity in central Utah has changed significantly since 1986, when wastewater injection started, we plotted the cumulative seismicity of the study four areas over time. Figure 2 shows that Areas 1 and 2 have had a nearly constant seismicity rate since 1981, indicating that seismicity in these areas are not affected by wastewater injection, which was substantial. Area 1 (Fig. 2A) has nineteen wastewater disposal wells,

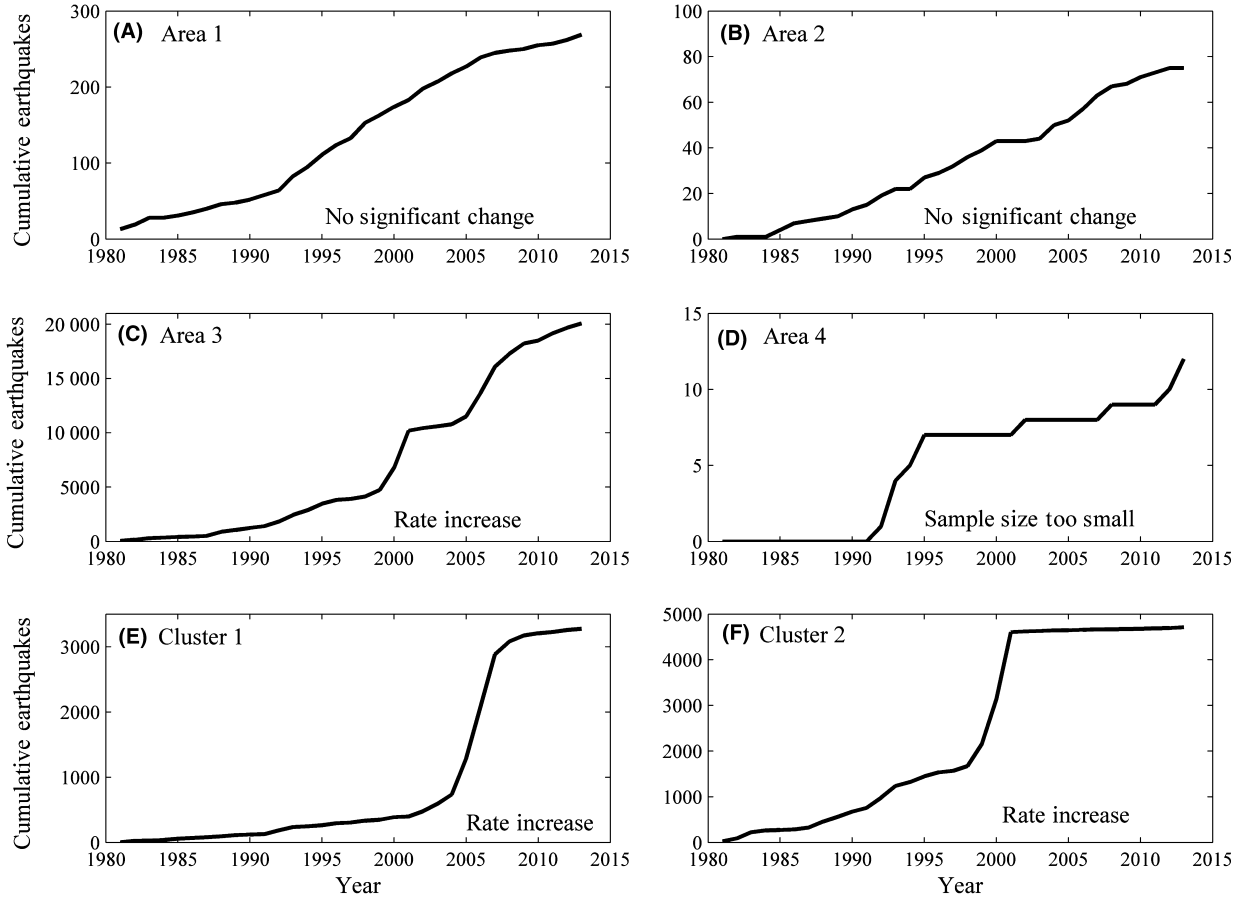

Fig. 2. Cumulative seismicity over time since 1981 for the areas of interest. Slope of the curves is the seismicity rate.

including seven active, of which at least two have been active since 1980s (UIC public record well files). The wells have injected approximately 2.44×10^8 barrels (bbls) (2.93×10^7 m^3) of wastewater as of October 2014 (UIC public record well files). Area 2 (Fig. 2B) has 80 wastewater disposal wells, 61 of which are active, and 1265 active water injection wells used for enhanced recovery (UIC public record well files). The total injected volume from the 80 wastewater disposal wells is 6.3×10^8 bbls (7.56×10^7 m^3) as of January 2015 (UIC public record well files). Injections in these areas had no significant impact on seismicity, so we will not examine data from these two areas. We will also exclude data from Area 4 – although it shows changes of seismicity rates, the rate is too low there to determine whether it is collocated with injection or not (Fig. 2D).

Area 3 has had >18 000 seismic events (magnitudes ranging −0.84 to 5.17) and clear changes of seismicity rate since 1981 (Fig. 2C). We chose two subregions of Area 3, Cluster 1 and Cluster 2, based on the spatial clustering of seismicity and injection wells (Fig. 1B), to further examine the changes in seismicity rates. The clusters were chosen to center around the wells of interest and seismicity directly adjacent to the wells, particularly in the direction of regional groundwater flow (Hood & Patterson 1984). Both subregions show clear increase in seismicity rate after the injection (Fig. 2E,F).

The concept of magnitude of completeness, M_c, the minimum magnitude of complete earthquake record in a catalog, is a concept based on the assumption of a power-law relationship between magnitude and number of events (Wiemer & Wyss 2000; Woessner & Wiemer 2005). This assumption fails at the two ends, with the smallest events and the largest events. Choosing a conservative M_c can cause an under sampling of events, especially in the events of interest at the lower magnitudes. We calculated a conservative M_c based on the maximum curvature method (Wiemer & Wyss 2000; Woessner & Wiemer 2005), which defines the magnitude of completeness as the point of maximum curvature in the frequency–magnitude curve. This point often matches the highest frequency magnitude bin in the noncumulative frequency–magnitude distribution. The magnitude–frequency distribution of earthquakes is based on the power-law equation:

$$\log_{10} N = \mathrm{a} - \mathrm{b}M \tag{1}$$

where M is the magnitude, N is the number of observed events greater than or equal to magnitude M, and a and b are constants (Gutenberg & Richter 1944). Figure 3 shows the frequency–magnitude distribution for pre- and post-injection in Area 3, Cluster 1, and Cluster 2 in both cumulative event and noncumulative event form. A conservative M_c for the entire time span of the study is M2.0. When the seismicity rates of Area 3 and Clusters 1 and 2

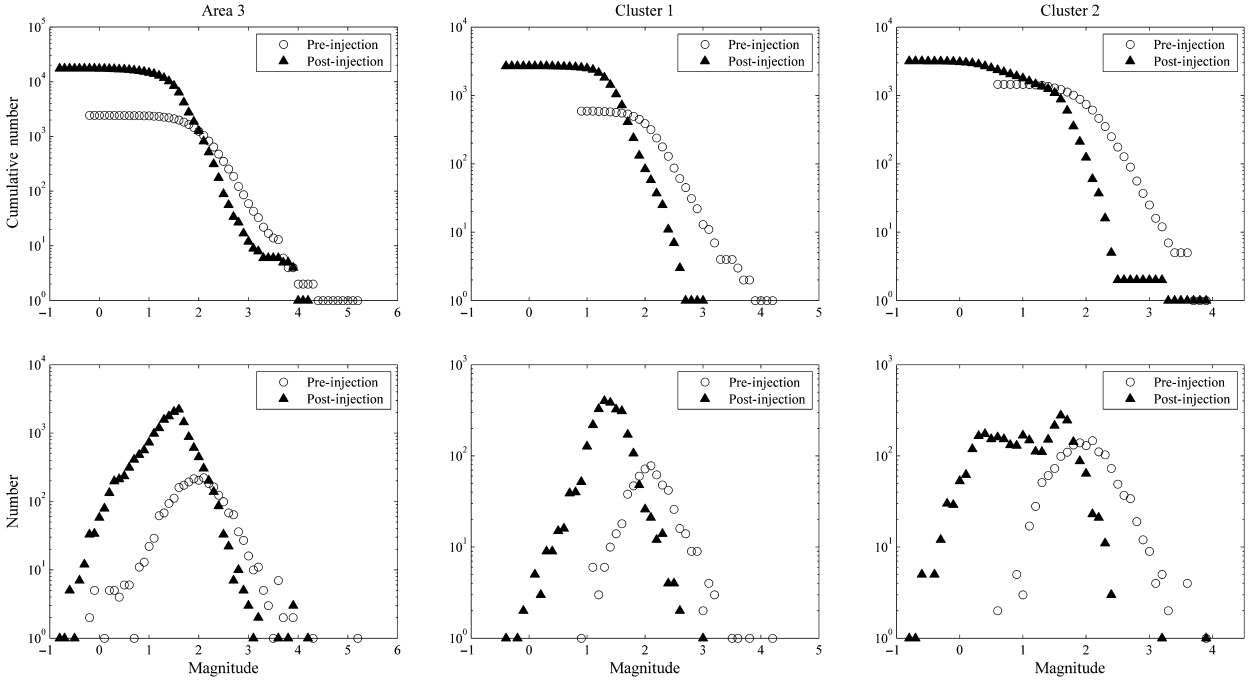

Fig. 3. Cumulative frequency–magnitude distribution of events and number of events of each magnitude bin for Area 3, Cluster 1, and Cluster 2 pre- and post-injection. Magnitudes are binned in intervals of 0.1. Open-dots are pre-injection data, and filled triangles are post-injection data.

are plotted with only events over the conservative M_c as in Fig. 4, the rates change.

CORRELATIONS WITH MINING AND INJECTION

Because of abundant seismicity and clear change of seismicity rates in the Area 3, we focus on this area to further explore the potential correlation between the seismicity and mining activity and wastewater injection. Area 3 has 32 active wastewater disposal wells, 27 of which inject into the Navajo Sandstone, Kayenta Formation, and Wingate Sandstone (UIC public record well files) since 1996. These formations are considered one hydrogeological unit in the area, the Navajo aquifer (Freethey & Cordy 1991). We removed the volumes injected into other formations in the wells that first injected into formations other than the Navajo aquifer. Cluster 1 takes into account the well volumes of five wells of interest that inject into the Navajo aquifer, and Cluster 2 takes into account the well volumes of three wells that inject into the Navajo aquifer.

Figure 5 compares the temporal variation of the rate of seismicity with that of mining activity and injection. For Area 3 as a whole, significant increases of seismicity rates occurred a couple of years after the beginning of wastewater injection, while the mining activity kept a similar rate, which actually decreased since around 2001 (Fig. 5A). This is clearer from the comparison of annual rates. Although the peaks of seismicity show strong correlation with mining activity (Fig. 5B), the correlation of the peak of seismicity between 2006 and 2010 with mining activity may be artificial – mining induced seismicity should be concurrent with mining activity, but there is an approximately 1-year shift in the temporal correlation. On the other hand, the two

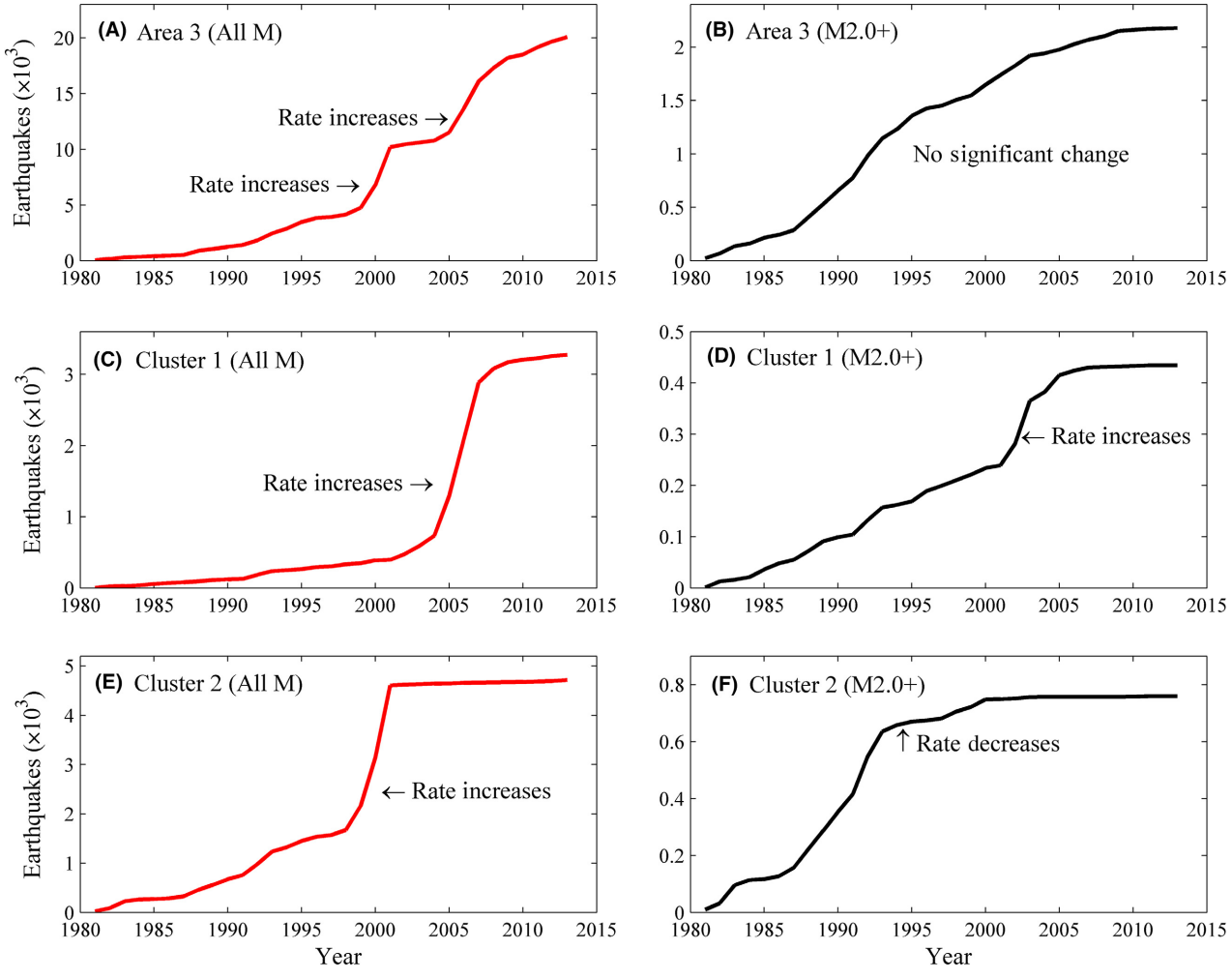

Fig. 4. Cumulative seismicity over time since 1981 for all earthquakes and earthquakes above the conservative M_c 2.0. Area 3 (A & B) shows an increased seismicity rate with all earthquakes and no significant rate changes when using a conservative M_c. Cluster 1 (C & D) shows an increased seismicity rate with all earthquakes and continues to show an increase in seismicity rate, although a more subdued one, when using a conservative M_c. Cluster 2 (E & F) shows an increased seismicity rate with all earthquakes and a decrease in seismicity over the conservative M_c.

peaks of seismicity since 1998 are clearly correlated with wastewater injection, and the approximately 2 year-lag between the peak of seismicity and the beginning of injection is consistent with the time needed for pore pressure diffusion to induce earthquakes.

Similar correlations are observed in the subregions of Cluster 1 and Cluster 2. In both areas, seismicity rates increased sharply after injection began (Fig. 5D and G). Whereas seismicity rates show strong temporal correlations with both mining activity and wastewater injection, mining alone cannot explain the time shift between the peak seismicity and mining activity (Fig. 5B and E). Neither can it explain the drastic decrease in seismicity after 2004 in Cluster 2 (Fig. 5H), while mining activity has continued. The correlations do become less clear if only events above the conservative M_c value are used.

To investigate the spatial distribution of the seismicity and its potential correlation with wastewater injection, we calculated and plotted the surface distance between each seismic event and the center point of the cluster of wastewater disposal wells for Clusters 1 and 2 (Fig. 6). Before injection, the seismicity was scattered over a large range of distances from the wells. After the injection, the seismicity in both areas seems to be clustered between 10 and 12 km from the well cluster center. This clustering is observed when the evaluation uses all the seismic events or only the events above the conservative M_c value.

PORE PRESSURE CHANGES BY INJECTION

We tested whether or not injection could have raised pore pressure sufficiently to cause the increased seismicity in Area 3. Increase in the Coulomb stress by more than 0.01 MPa is needed to cause statistically significant increase in seismicity rates (King *et al.* 1994), which implies an increase in the hydraulic head by 1 m or more for pore pressure to be the cause. Hence, the test is to see whether injection in Area 3 could raise the hydraulic head

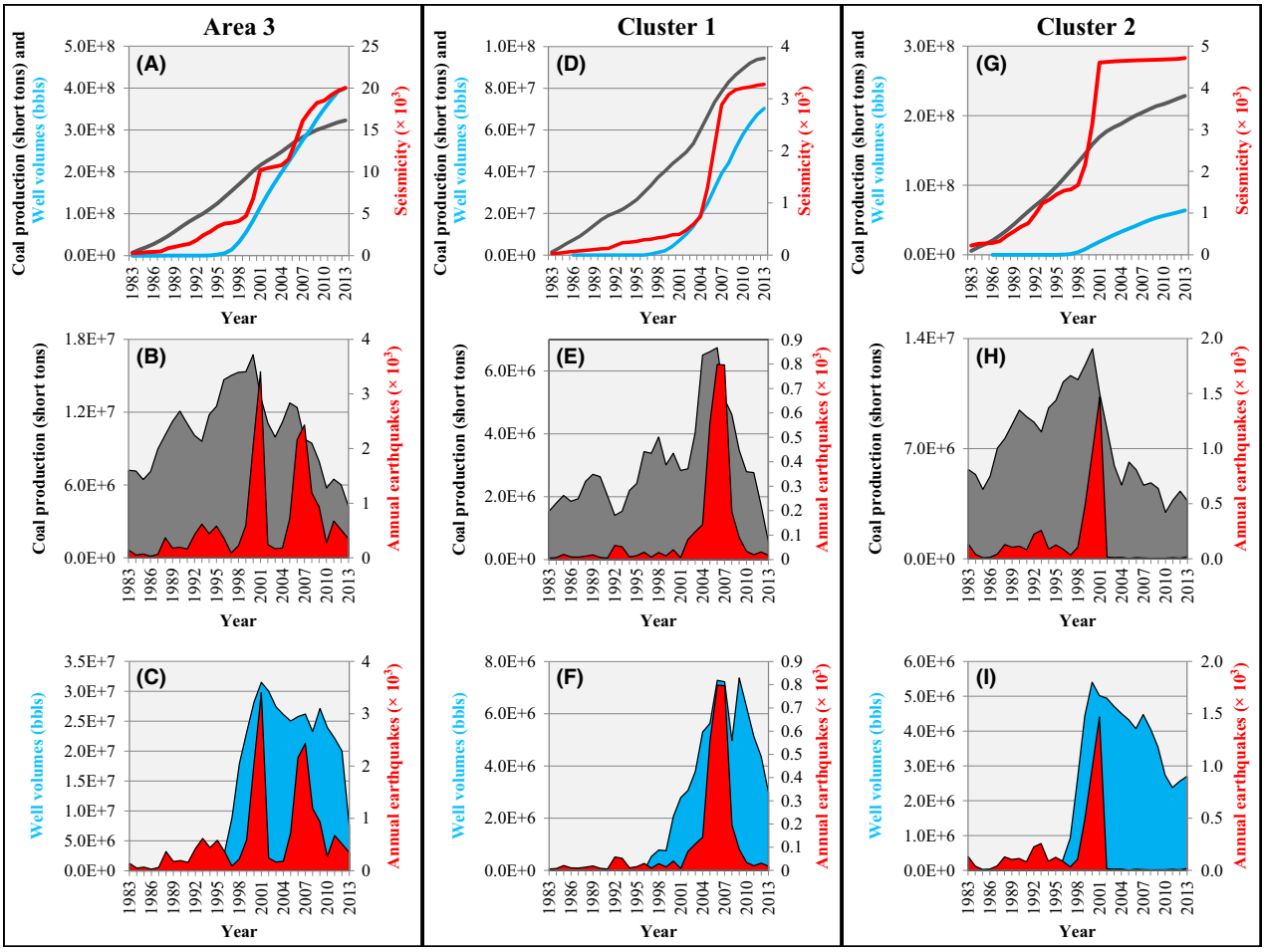

Fig. 5. Temporal correlation between seismicity (red), wastewater injection volumes (blue), and coal production (gray) for Area 3, Cluster 1, and Cluster 2. Axes labels are color coded to match the data displayed. (A, D, and G) Seismicity rates, injection rates, and coal production rates for Area 3 as a whole, and Clusters 1 and 2. (B, E, and H) Annual coal production and earthquake totals. (C, F, and I) Annual wastewater injection volumes and earthquake totals.

by 1 m or more within 1–5 years after injection started and over a distance 10–12 km from the injection wells, as indicated by the spatiotemporal patterns of seismicity and injection (Fig. 5).

Theis (1935) provides an analytical solution for change in hydraulic head as a result of a pumping or injection well in a homogeneous, isotropic aquifer:

$$\Delta h(r,t) = \frac{Q}{4\pi T}\int_{u}^{\infty}\frac{e^{-x}\mathrm{d}x}{x} \tag{2}$$

where $u = r^2S/4Tt$ is dimensionless time parameter, Q is the injection rate, T and S are the transmissivity and storativity, r is the distance from the well, x is the variable of integration, and t is the time since injection began. The Theis solution assumes an infinite, flat confined aquifer of constant thickness, which is homogenous and isotropic. While these assumptions do not accurately represent the Navajo aquifer, the Theis solution gives a first-order result for pore pressure change under the average injection conditions. We calculated the change in hydraulic head for a constant injection rate of 1370 m^3 day^{-1} for 10 years (Fig. 7). This rate of injection is three times the average injection rate in Area 3 to represent the three injection wells in Area 3's Cluster 2. We tested a range of transmissivity and storativity values based on properties of the Navajo Sandstone, which makes up the majority of the aquifer (Hood & Danielson 1979; Hood & Patterson 1984; Freethey & Cordy 1991).

Figure 7A is an example graph explaining how to read the results, and Fig. 7B presents the results of the Theis solution. As shown in Fig. 7B, low transmissivity and low storativity promote raising pore pressure. With $T < 400$ m^2 day^{-1} and $S < 0.0003$, the injection could have raised the hydraulic head more than 1 m over a distance 10–12 km from the wells within 10 years after injection (Fig. 7B(i) and (iii)). For $T > 125$ m^2 day^{-1} and $S > 0.008$, hydraulic head increase is less than a couple of meters and within 2–4 km from the wells (Fig. 7B(ii) and (iv)). The ranges of the transmissivity and storativity in Fig. 7 are based on the values of the Navajo aquifer (Freethey & Cordy 1991); these results suggest that the wastewater injection could cause the increased seismicity in Area 3.

To more accurately represent the Navajo aquifer with the injection area's shallow dip, we also modeled the change of hydraulic head by injection using the Groundwater Modeling System (GMS), which provides a graphical user interface for the MODFLOW 2000 model. MODFLOW solves the transient groundwater flow equation (McDonald & Harbaugh 1988):

$$S_s\frac{\partial h}{\partial t} = \frac{\partial}{\partial x}\left(K_{xx}\frac{\partial h}{\partial x}\right) + \frac{\partial}{\partial y}\left(K_{yy}\frac{\partial h}{\partial y}\right) + \frac{\partial}{\partial z}\left(K_{zz}\frac{\partial h}{\partial z}\right) + W \tag{3}$$

where S_s is specific storage of the aquifer, h is hydraulic head, t is time, K is hydraulic conductivity along the indicated coordinate axes x, y, or z, and W is the volumetric flux per unit volume representing sources and/or sinks of water (such as an injection well).

We built an isotropic, homogeneous, one-layer grid model dipping 3°, based on the mapped dip for the area (Witkind 1988); the model domain is 250 m thick (Fig. 8). In this model, the z-component of the transient groundwater flow equation is zero. To minimize the impact the poorly constrained lateral boundary conditions, we use a large 80 km by 80 km model domain. The numerical grid is 250 m by 250 m by 250 m. In this

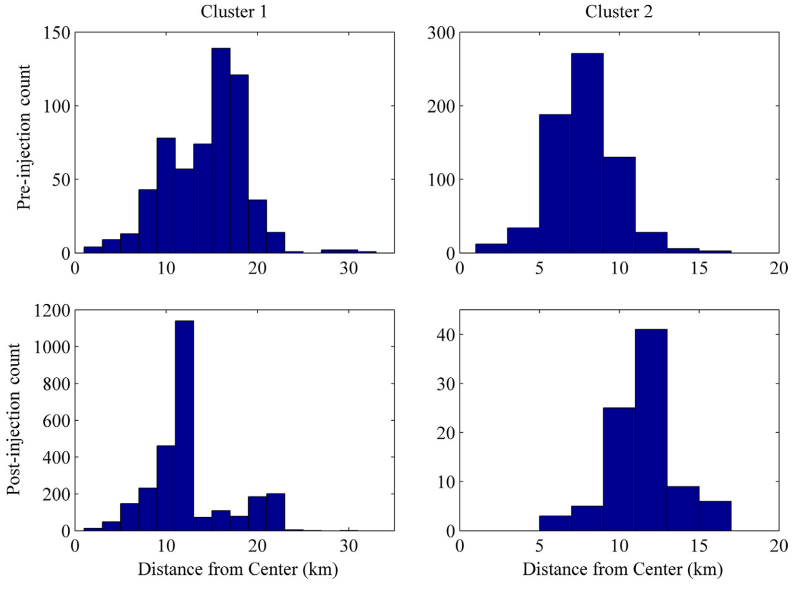

Fig. 6. Surface distance of seismicity pre- and post-injection as measured from the cluster centers of Cluster 1 and Cluster 2.

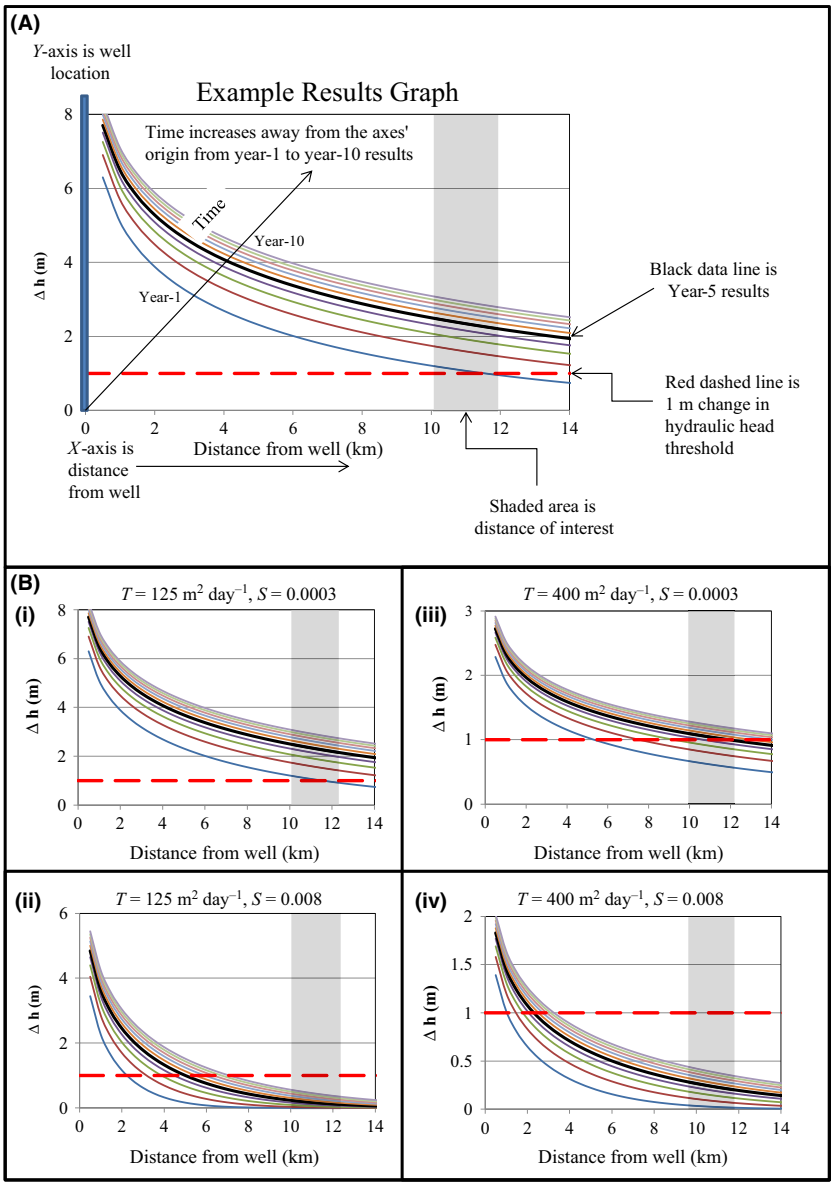

Fig. 7. Theis solution (analytical) results. (A) Example results describing the parts of the graph and how to read the results. (B) Theis solution results with change in hydraulic head (Δh), in meters, as a function of distance from the injection well, in kilometers, in homogeneous, isotropic aquifers with a single injection well with a constant injection rate of 1370 m^3 day^{-1}. The location $X = 0$, and therefore the *y*-axes, represents the location of the injection well and time increases away from the origin of each graph, with each line representing the Δh for each successive year of injection up to 10 years. The black lines are the 5 years of injection change in hydraulic head data. Red dashed lines represent the 1 m change in hydraulic head threshold, which can induce seismicity. The gray areas are the distances of interest, approximately 10–12 km from the injection well. Transmissivity (T) values and storativity (S) values are (i) T = 125 m^2 day^{-1}, S = 0.0003; (ii) T = 125 m^2 day^{-1}, S = 0.008; (iii) T = 400 m^2 day^{-1}, S = 0.0003; and (iv) T = 400 m^2 day^{-1}, S = 0.008.

semi-generic model, a single injection well was located in the center of the model domain with a constant injection rate of 1370 m^3 day^{-1}. The single well is used to approximate the injection in the actual aquifer using a rate three times the average rate of the injection wells of interest. We set the model as a confined aquifer and used hydrostatic pressure as the initial condition. Hydrostatic conditions are also applied to the lateral boundaries to allow groundwater flowing out of the model domain.

We ran the model with four hydraulic conductivity (K) values (0.001 m day^{-1}, 0.01 m day^{-1}, 0.5 m day^{-1}, and 1.6 m day^{-1}) and at two specific storage (S_s) values (1.2×10^{-6} m^{-1} and 3.2×10^{-5} m^{-1}) each. For the dipping aquifer, the greatest change in hydraulic head is in the down-dip direction in which the natural hydraulic gradient is also the greatest. The results in Fig. 9 are those in the down-dip direction. Figure 9 presents the results in terms of transmissivity and storativity, which are K and S_s multiplied by the aquifer thickness (250 m), respectively. The results graphs in Fig. 9 can be interpreted in the same manner as the example in Fig. 7A.

Figure 9 shows the results are similar to those of the analytic model – low to mid-range transmissivity and low storativity help to raise pore pressure. Within the estimated range of the transmissivity and storativity for the Navajo aquifer (Hood & Danielson 1979; Hood & Patterson 1984; Freethey & Cordy 1991), injection is shown to be able to raise hydraulic head more than 1 m over a region up to 10–12 km from the injection wells to account for the observed seismicity increase.

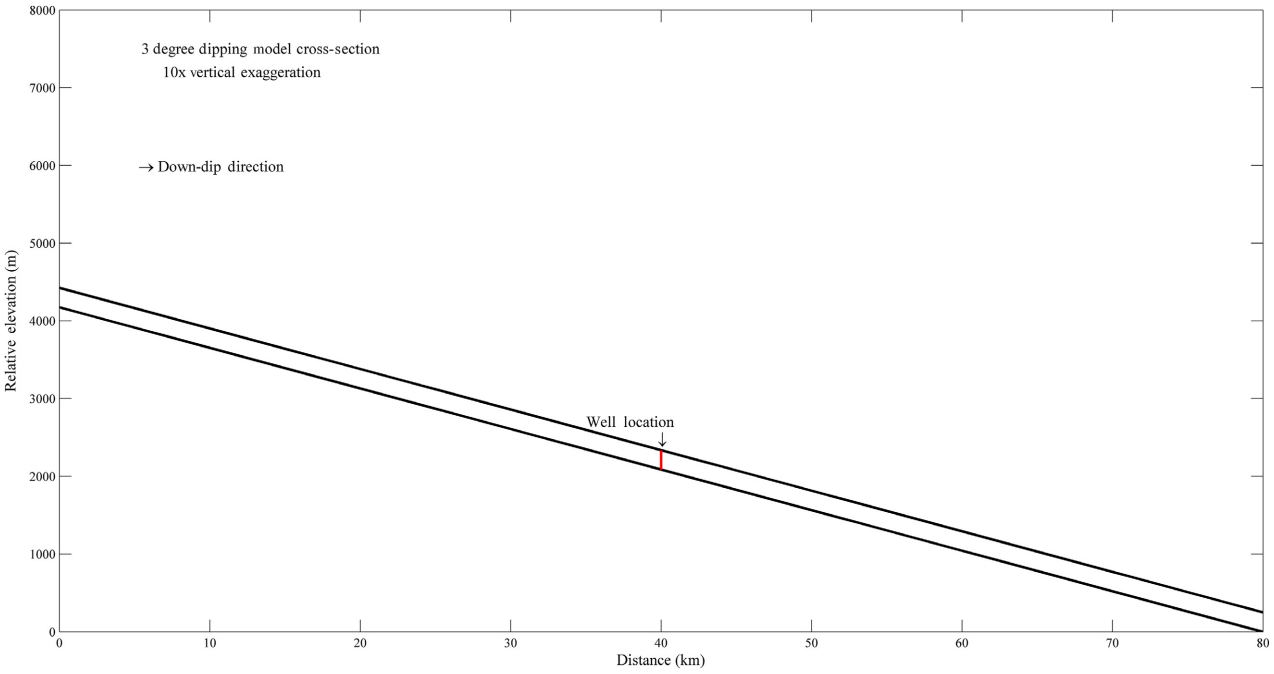

Fig. 8. Cross-sectional view of the numerical model domain. This line drawing is shown with 10 times vertical exaggeration. The 3° dipping model is 250 m thick and spans 80 km by 80 km in map view (not shown). The well is located in the center of the model domain (shown in red). Results of the model are shown in the down-dip direction in a later figure.

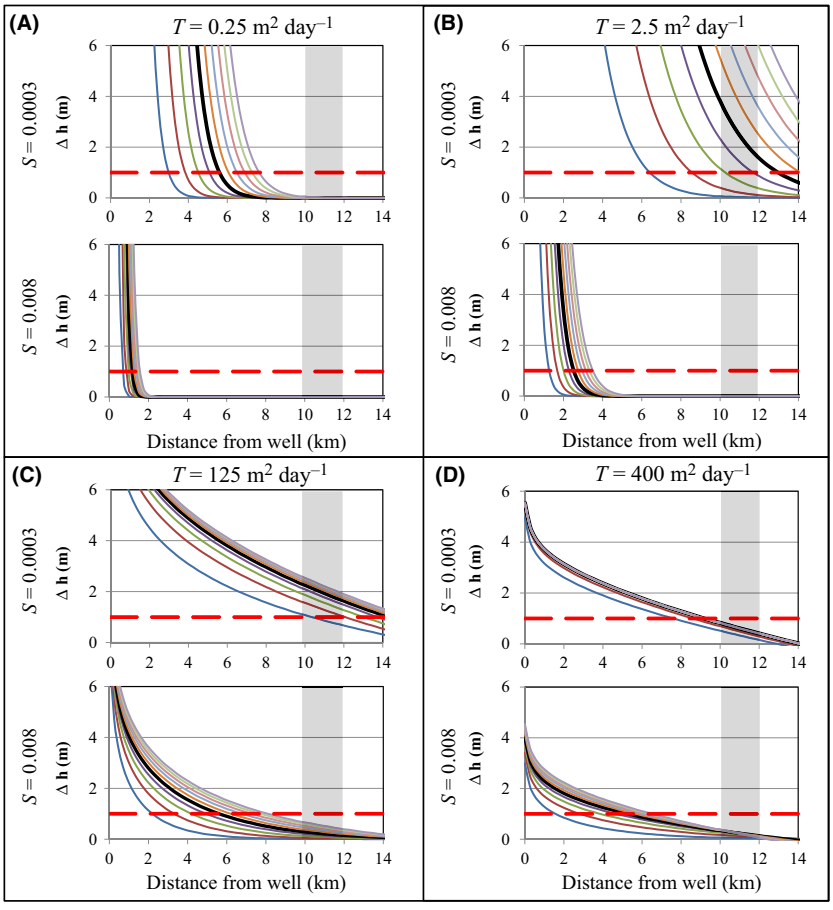

Fig. 9. Model results for a 3° dipping, numerical model; distance from the injection well is in the down-dip direction. Result graphs can be read as described in Fig. 7A. Change in hydraulic head (Δh), in meters, as a function of distance from the injection well, in kilometers, in a homogeneous, isotropic aquifer with a single injection well with a constant injection rate of 1370 m^3 day^{-1}. The location $X = 0$, and therefore the y-axes, represents the location of the injection well and time increases away from the origin of each graph, with each line representing the Δh for each successive year of injection up to 10 years. The black lines are the 5 years of injection change in hydraulic head data. Red dashed lines represent the 1 m change in hydraulic head threshold, which can induce seismicity. The gray areas are the distances of interest, approximately 10–12 km from the injection well. Transmissivity values are (A) 0.25 m^2 day^{-1}, (B) 2.5 m^2 day^{-1}, (C) 125 m^2 day^{-1}, and (D) 400 m^2 day^{-1}, and the storativity values are 0.0003 (first row) and 0.008 (second row) for each panel (A–D).

Table 1 *b*-value and uncertainty.

Area	Pre-injection	Pre-injection uncertainty	Post-injection	Post-injection uncertainty
Area 3	1.12	0.03	2.00	0.06
Cluster 1	1.25	0.05	1.95	0.18
Cluster 2	1.23	0.04	2.65	0.32

Nomenclature

Symbol	Units	Description
Theis and Groundwater Flow Equations		
Δh	[m]	Change in hydraulic head, drawdown
r	[m]	Radial distance from well
t	[d]	Time
Q	[m^3 day^{-1}]	Volumetric injection rate
u	[1]	Dimensionless time parameter
T	[m^2 day^{-1}]	Transmissivity of the confined aquifer
S	[1]	Storativity of the confined aquifer
K	[m day^{-1}]	Hydraulic conductivity of the confined aquifer
S_s	[m^{-1}]	Specific storage of the confined aquifer
b-value calculations		
M	[1]	Earthquake magnitude
N	[1]	Number of observed events greater than or equal to magnitude M
a	[1]	Constant
b	[1]	Constant; *b*-value
M_c	[1]	Magnitude of completeness
ΔM	[1]	Magnitude interval used for grouping of the data
$\hat{\mu}$	[1]	Sampling average of the magnitudes
σ	[1]	*b*-value uncertainty
σ_m	[1]	Modified *b*-value uncertainty

CHANGES IN *B*-VALUE

Injection-induced earthquakes have a fundamentally different mechanism than mining induced seismicity. As differential stress and *b*-value have an inverse relationship, *b*-value can be used as a stress indicator (Schorlemmer *et al.* 2005).

The *b*-value characterizes the magnitude–frequency distribution of earthquakes presented in Eq. 1 (Gutenberg & Richter 1944). A *b*-value of 1 is the global average for tectonic earthquakes, while injection-induced earthquakes have larger *b*-values (National Research Council of the National Academies 2013). Seismicity in Area 3 has long been considered entirely MIS, with only extremely rare tectonic events. Therefore, prior to injection, all the seismicity is mining induced. Relatively higher *b*-values have been observed in other fluid influenced environments like volcanic areas (Wiemer & McNutt 1997), hydrothermal areas (Farrell *et al.* 2009) and geothermal areas (Bachmann *et al.* 2012). Figure 3 presents the cumulative frequency magnitude distribution of events and the noncumulative frequency magnitude distribution of events for Area 3, Cluster 1, and Cluster 2 pre- and post-injection.

We evaluated temporal variation in the *b*-value for pre- and post-injection using a modified maximum likelihood estimation that takes into account the binning process (Aki 1965; Utsu 1965; Bender 1983; Marzocchi & Sandri 2003). The formula for *b*-value is

$$b = \frac{1}{\ln(10)\left[\hat{\mu} - \left(\frac{2M_c - \Delta M}{2}\right)\right]} \tag{4}$$

where $\hat{\mu}$ is the sampling average of the magnitudes, M_c is the magnitude of completeness, and ΔM is the magnitude interval used for grouping of the data. A ΔM value of 0.1 is used for instrumental measurements (Marzocchi & Sandri 2003), and this value was used for our estimations. Uncertainty in *b*-value calculations is estimated by a formula modified from the original (Aki 1965):

$$\sigma = \frac{b}{\sqrt{N}} \tag{5}$$

where N is the number of earthquakes. The modified formula we used is

$$\sigma_m = 2.30b^2\sqrt{\frac{\sum_{i=1}^{N}(M_i - \hat{\mu})^2}{N(N-1)}} \tag{6}$$

where σ_m is the modified uncertainty and N is the number of earthquakes. The *b*-values and uncertainties calculated using a M_c of 2.0 are presented in Table 1. In Area 3, Cluster 1, and Cluster 2 the *b*-value increases following the start of consistent injection. We also calculated the *b*-values using lower M_c values, and while the magnitude of the *b*-values changed, the increase in *b*-value following the start of injection remained regardless of the chosen M_c value.

DISCUSSION

The variations of seismicity rates after consistent injection in central Utah show clearly that not all injections induce seismicity (Fig. 2), as has been observed elsewhere (Ellsworth 2013). This may be explained by either insufficient amount of injection, or the stress state in the crust that is far from the failure conditions, or a combination of both factors. In Area 1, approximately 2.44×10^8 bbls (2.93×10^7 m^3) of wastewater has been injected by

October 2014 (UIC public record well files), which is approximately 61% of the amount injected into Area 3. The relatively low injection volume could be a factor for the lack of induced seismicity in Area 1. In Area 2, the total injected volume from 80 wastewater disposal wells is 6.3×10^8 bbls (7.56×10^7 m^3) as of January 2015 (UIC public record well files), approximately 1.6 times the amount injected into Area 3. Therefore, the lack of injection-induced seismicity there has to be explained by other factors, perhaps including it being located away from the Intermountain Seismic Zone so the stress in the ambient crust is too low for injection-induced seismicity. As for Area 4, the total volume injection, about 3.3×10^7 bbls (3.96×10^6 m^3) (UIC public record well files), is approximately 8.3% of the volume injected in Area 3. Although the area shows some variation in seismicity rate since 1981, the small sample size does not permit meaningful analysis.

Our analysis focused on seismicity changes in Area 3, where seismicity increased significantly since the injection. Previous studies have attributed all seismicity in the area to mining activity (Arabasz & Pechmann 2001; Arabasz *et al.* 2005, 2007). Although mining is clearly a major cause of the induced seismicity in central Utah (Arabasz *et al.* 2002), we cannot explain the significant increase in seismicity during the 2000s by the mining activity alone. First, although mining in Area 3 has been active since well before the 1980s, the significant increase in seismicity started only after the consistent injection began around 1998 (Fig. 5). Second, whereas the peak seismicity rate seems temporally correlated with peak mining activity, the 1–2 year shift between them indicate other processes are involved, because mining induced seismicity should be coeval with mining activity. On the other hand, the peak seismicity rate also correlate well with injection volumes (Fig. 5), and the time shifts between them can be explained by the time needed for pore pressure diffusion to trigger earthquakes. Finally, the increased seismicity appears to cluster at specific distances (Fig. 6) from the wells, which would be consistent with pore pressure induced seismicity along preexisting faults. The clustering distance is close to the coal mines and could be due to coal mining activity; however, the variable spatial pattern prior to injection when coal mining was also active suggests the change is due to another process.

Our results of *b*-values of these seismic events are comparable with previous studies for the Utah mining region (Smith *et al.* 1974; Pechmann *et al.* 2008; Kubacki *et al.* 2014). These calculations, however, were completed over two years or less. The *b*-values we calculated for Area 3, Cluster 1, and Cluster 2 (Fig. 7) spanned at least 9 years. Our results show temporal and spatial variations. Prior to injection, Area 3 and the two clusters have *b*-values approximately the same and slightly higher than the tectonic average of 1. This *b*-value represents only MIS. Following the start of injection, Area 3, Cluster 1, and Cluster 2 show an increase in *b*-value. The increase in *b*-value following the start of injection is consistent with changes in differential stress (Schorlemmer *et al.* 2005), which is consistent with a change from exclusively MIS to a mix of MIS and injection-induced seismicity.

CONCLUSIONS

We conclude that not all injection in central Utah has induced seismicity. In Area 2 of our study area, in the Uinta Basin area of central Utah, where 6.3×10^8 bbls (7.56×10^7 m^3) wastewater has been injected in 80 wells from the mid-1960s to January 2015, no clear increase in seismicity has been found.

On the other hand, we find strong evidence for injection-induced seismicity in Area 3. Our analysis confirms that much of the increased seismicity is related to coal mining, but mining activity alone cannot explain the significant increase in seismicity since 2000, and the increased seismicity can be better explained with additional seismicity induced by wastewater injection. The injection-induced seismicity apparently clusters on preexisting faults, indicating that tectonic conditions are a key factor even for induced seismicity.

REFERENCES

Aki K (1965) Maximum likelihood estimate of *b* in the formula $\log(N) = a - b$M and its confidence limits. *Bulletin of Earthquake Research Institute, Tokyo University*, **43**, 237–9.

Arabasz WJ, Pechmann JC (2001) Seismic characterization of coal-mining seismicity in Utah for CTBT monitoring, *Technical Report UCRL-CR-143772*, LLNL Research Agreement No. B344836, Livermore, California.

Arabasz WJ, Nava SJ, McCarter MK, Pankow KL (2002) Ground-Motion Recording and Analysis of Mining-Induced Seismicity in the Trail Mountain Area, Emery County, Utah: Final Report for State of Utah School and Institutional Trust Lands Administration.

Arabasz WJ, Nava SJ, McCarter MK, Pankow KL, Pechmann JC, Ake J, McGarr A (2005) Coal-mining seismicity and ground-shaking hazard: a case study in the trail mountain area, Emery County, Utah. *Bulletin of the Seismological Society of America*, **95**, 18–30.

Arabasz WJ, Burlacu R, Pankow KL (2007) An overview of historical and contemporary seismicity in central Utah. In: *Central Utah – Diverse Geology of a Dynamic Landscape* (eds Willis GC, Hylland MD, Clark DL, Chidsey TC), pp. 236–53. Utah Geological Association Publication, Salt Lake City.

Bachmann CE, Wiemer S, Goertz-Allmann BP, Woessner J (2012) Influence of pore-pressure on the event-size distribution of induced earthquakes. *Geophysical Research Letters*, **39**, L09302.

Bender B (1983) Maximum likelihood estimation of b values for magnitude grouped data. *Bulletin of the Seismological Society of America*, **73**, 831–51.

Ellsworth WL (2013) Injection-induced earthquakes. *Science*, **341**, 1225942. doi:10.1126/science.1225942.

Farrell J, Husen S, Smith RB (2009) Earthquake swarm and *b*-value characterization of the Yellowstone volcano-tectonic system. *Journal of Volcanology and Geothermal Research*, **188**, 260–76.

Freethey GW, Cordy GE (1991) Geohydrology of mesozoic rocks in the upper Colorado River Basin in Arizona, Colorado, New Mexico, Utah, and Wyoming, excluding the San Juan Basin. In: *Regional Aquifer-System Analysis – Upper Colorado River Basin, Excluding San Juan Basin*. US Geological Survey Professional Paper 1411-C: Washington, DC, USA.

Gutenberg B, Richter CF (1944) Frequency of earthquakes in California. *Bulletin of the Seismological Society of America*, **34**, 185–8.

Hood JW, Danielson TW (1979) Aquifer tests of the navajo sandstone near Caineville, Wayne County, Utah. In: *State of Utah Department of Natural Resources Technical Publication No. 66, USA*.

Hood JW, Patterson D (1984) Bedrock aquifers in the northern San Rafael Swell area, Utah, with special emphasis on the Navajo Sandstone. In: *State of Utah Department of Natural Resources Technical Publication No. 78, USA*.

Keranen KM, Savage HM, Abers GA, Cochran ES (2013) Potentially induced earthquakes in Oklahoma, USA: links between wasterwater injection and the 2011 M_w 5.7 earthquake sequence. *Geology*, **41**, 699–702.

King GCP, Stein RS, Lin J (1994) Static stress changes and the triggering of earthquakes. *Bulletin of the Seismological Society of America*, **84**, 935–53.

Kubacki T, Koper KD, Pankow KL, McCarter MK (2014) Changes in mining-induced seismicity before and after the 2007 Crandall Canyon Mine collapse. *Journal of Geophysical Research: Solid Earth*, **119**, 4876–89.

Marzocchi W, Sandri L (2003) A review and new insights on the estimation of the *b*-value and its uncertainty. *Annals of Geophysics*, **46**, 1271–82.

McDonald MG, Harbaugh AW (1988) *A Modular Three-Dimensional Finite-Difference Ground-Water Flow Model: U.S. Geological Survey Techniques of Water-Resources Investigations*, book 6, chap. A1, 586 p.

McGarr A (2014) Maximum magnitude earthquakes induced by fluid injection. *Journal of Geophysical Research: Solid Earth*, **119**, 1008–1019.

National Research Council of the National Academies (2013) *Induced Seismicity Potential in Energy Technologies*, p. 300. The National Academies Press, Washington, DC.

Pechmann JC, Nava SJ, Terra FM, Bernier JC (2007) Local magnitude determinations for intermountain seismic belt earthquakes from broadband digital data. *Bulletin of the Seismological Society of America*, **97**, 557–74.

Pechmann JC, Arabasz WJ, Pankow KL, Burlacu R, McCarter MK (2008) Seismological report on the 6 August 2007 Crandall Canyon mine collapse in Utah. *Seismological Research Letters*, **79**, 620–36.

Schorlemmer D, Wiemer S, Wyss M (2005) Variations in earthquake-size distribution across different stress regimes. *Nature*, **437**, 539–42.

Smith RB, Winkler PL, Anderson JG (1974) Source mechanisms of microearthquakes associated with underground mines in eastern Utah. *Bulletin of the Seismological Society of America*, **64**, 1295–317.

Theis CV (1935) The relation between the lowering of the piezometric surface and the rate and duration of discharge of a well using ground water storage. *Transactions. American Geophysical Union*, **2**, 519–24.

Utsu T (1965) A method for determining the value of *b* in a formula log $n = a - bM$ showing the magnitude-frequency relation for earthquakes. *Geophysical Bulletin Hokkaido University, Hokkaido, Japan*, **13**, 99–103.

Wiemer S, McNutt SR (1997) Variations in the frequency-magnitude distribution with depth in two volcanic areas: Mount St. Hellens, Washington, and Mt. Spurr, Alaska. *Geophysical Research Letters*, **24**, 189–92.

Wiemer S, Wyss M (2000) Minimum magnitude of completeness in earthquake catalogs: examples from Alaska, the Western United States, and Japan. *Bulletin of the Seismological Society of America*, **90**, 859–69.

Witkind IJ (1988) Geologic Map of the Huntington 30′ × 60′ Quadrangle, Carbon, Emery, Grand, and Uintah Counties, Utah: U.S. Geological Survey, scale 1:100000.

Woessner J, Wiemer S (2005) Assessing the quality of earthquake catalogues: estimating the magnitude of completeness and its uncertainty. *Bulletin of the Seismological Society of America*, **95**, 684–98.